J Mater Sci: Mater Med (2010) 21:1047–1055
DOI 10.1007/s10856-009-3940-9

Biomineralization capability of adherent bio-glass films prepared by magnetron sputtering

G. E. Stan · S. Pina · D. U. Tulyaganov · J. M. F. Ferreira · I. Pasuk · C. O. Morosanu

Received: 11 June 2009 / Accepted: 6 November 2009 / Published online: 29 November 2009

Abstract Radiofrequency magnetron sputtering deposition at low temperature (150°C) was used to deposit bioactive glass coatings onto titanium substrates. Three different working atmospheres were used: Ar 100%, Ar + 7%O_2, and Ar + 20%O_2. The preliminary adhesion tests (pull-out) produced excellent adhesion values (~75 MPa) for the as-deposited bio-glass films. Bioactivity tests in simulated body fluid were carried out for 30 days. SEM–EDS, XRD and FTIR measurements were performed. The tests clearly showed strong bioactive features for all the prepared films. The best biomineralization capability, expressed by the thickest chemically grown carbonated hydroxyapatite layer, was obtained for the bio-glass coating sputtered in a reactive atmosphere with 7% O_2.

1 Introduction

Bioactive glass (BG) coatings are a promising alternative to the classical hydroxyapatite (HA) coatings. These materials were studied with preponderance in powder or bulk form and they are characterized by their intimate and rapid bond with living bone through the formation of a carbonated hydroxyapatite interface layer [1–8]. Compared to HA coatings, the bioactivity of BG films deposited onto titanium (Ti) substrates were reported in a few articles [9–17]. Only one of these BG related papers refer to magnetron sputtered films [9]. Generally, low values of adhesion for BG/Ti interfaces were published [9, 17, 18]. Such behavior might be due to significant mismatch in the thermal expansion coefficients (CTE) of bio-glass coating (~14–15 × 10^{-6}/°C) and titanium substrate (~9.2–9.6 × 10^{-6}/°C) [10, 18–20].

Radio-Frequency magnetron sputtering (RF-MS) is a very powerful technique which can be used in a wide range of applications. Its flexibility along with the low pressure operation and low substrate temperature rise made it an attractive technique to deposit various films on different substrates. Other important advantages are the ease of sputtering almost any compound, the high-purity of the films, ease of automation, excellent uniformity on large-area substrates and extremely high adhesion of films [21].

New compositions of bioactive glass were recently developed and tailored to obtain CTE close to those of Ti and its alloys [22–25]. In this paper we report the bioactive behavior of novel BG thin films featuring suitable $CTE_{200–400°C}$ (10.7 × 10^{-6}/°C) prepared by magnetron sputtering (MS) on titanium. The BG powder composition was based on the SiO_2–CaO–MgO system along with P_2O_5, CaF_2, B_2O_3, and Na_2O as additives. The overall composition (wt%) is: SiO_2—40.08, CaO—29.1, MgO—8.96, P_2O_5—6.32, CaF_2—5.79, B_2O_3—5.16, and Na_2O—4.59 [7].

This paper concerns with the influence of RF-MS working atmosphere upon the biomineralization capability of the films after 30 days immersion in simulated body fluid (SBF), which is essential for biomedical applications [26]. It is known that the prerequisite for biomaterials to bond to living tissues is the formation of a crystalline HA

C. O. Morosanu: Deceased.

G. E. Stan (✉) · I. Pasuk · C. O. Morosanu
National Institute of Materials Physics, P.O. Box MG-7, Bucharest-Magurele 077125, Romania
e-mail: george_stan@infim.ro

S. Pina · D. U. Tulyaganov · J. M. F. Ferreira
Department of Ceramics and Glass Engineering, CICECO, University of Aveiro, Aveiro, Portugal

layer on their surfaces in physiological media which significantly enhances their biocompatibility by promoting osteosynthesis [19].

2 Materials and methods

2.1 Powder preparation

Powders of technical grade (purity >99.5%) silicon oxide and calcium carbonate, and of reagent grade of H_3BO_3, $4MgCO_3{\cdot}Mg(OH)_2{\cdot}5H_2O$, Na_2CO_3, CaF_2, and $NH_4H_2PO_4$ were used for BG preparation. Homogeneous mixtures of batches ($\sim$100 g), obtained by ball milling were preheated at 1000°C for 1 h for decarbonization and then melted in Pt crucibles at 1400°C for 1 h, in air. Frit glasses were obtained by quenching the melts into cold water. To obtain fine powders, the frits were dried and then milled in a high-speed porcelain mill. The mean particle size of the powders, calculated by the particle size distribution curves obtained by light scattering technique (Coulter LS 230, UK, Fraunhofer optical model), was about 11–14 μm.

2.2 Deposition procedure

High purity (99.6%) commercial titanium plates (Mateck GmbH) of 10 × 15 mm and glass (Corning) were used as substrates. Before deposition, the substrates were ultrasonically cleaned for 15 min in acetone and ethanol and then dried in nitrogen flow.

The BG films were prepared using a UVN-75R1 1.78 MHz sputtering deposition system having a magnetron cathode with a plasma ring of $\sim$55 mm diameter. The magnetron cathode target (110 mm diameter, 3 mm thick) was obtained by mild pressing of the BG powder at room temperature.

The sputtering chamber was first evacuated to a pressure lower than 3×10^{-3} Pa. Then spectral argon and oxygen were admitted through needle valves at various flows in order to obtain the desired deposition atmospheres of various oxygen dilutions, maintaining the total pressure constant. During the sputtering process the pressure was measured by a capacitive gauge (Alcatel ASD 1004). A constant argon volume flow rate of 45 sccm was used for all depositions, and three different working atmospheres (one inert and two reactive) were used: Ar 100%, and Ar + 7%O_2, Ar + 20%O_2, respectively (Table 1). Before deposition, the substrates were plasma etched in argon atmosphere for around 10 min in order to improve films adhesion.

The sputtering of BG/Ti coatings was carried out for around 1 h at a constant pressure of 0.3 Pa, using a target to substrate distance of 30 mm. During deposition the substrate heats due to the Ar plasma bombardment reaching a maximum temperature of 150°C, measured with a chromel–alumel thermocouple.

2.3 In vitro analysis in simulated body fluid

The in vitro bioactivity of the as-sputtered samples, reflected in their capability of inducing HA-formation onto their surfaces, was investigated by immersion in SBF at 37°C for 30 days. The SBF has the following composition, expressed in ionic concentrations (in mmol/dm^3): 142.0 Na^+, 5.0 K^+, 2.5 Ca^{2+}, 1.5 Mg^{2+}, 147.8 Cl^-, 4.2 HCO_3^-, 1.0 HPO_4^{2-} and 0.5 SO_4^{2-}, buffered at pH = 7.25 with tris-hydroxymethyl-amminomethane (Tris, 50 mmol/dm^3) and hydrochloric acid solutions according to Kokubo [27]. The SBF was filtered through sterilized filters (cameo 25 AS-MSI, pore size 0.22 μm). Sterilized glass flasks were used for the experiments. The volume of SBF used per sample was 10 ml and the SBF solution was not renewed during the experiment. Three replicates per sample were performed. Sampling took place at 30 days and the capability of inducing HA formation onto the coated surfaces was evaluated by SEM, XRD and FTIR measurements.

2.4 Characterizations of sputtered bio-glass coatings

a. The bio-glass layer thickness was estimated from optical spectroscopy transmittance by the Swanepoel procedure for films deposited on glass substrates, by using a UV–VIS–NIR *PerkinElmer Lambda 90* spectrophotometer. The transmittance measurements were performed in the wavelength range from 300 to 800 nm.
b. The crystallographic structure of each film was determined by X-ray diffraction, using a *Bruker D8*

Table 1 Deposition conditions of bio-glass films

Sample lot	Working atmosphere	Pressure (Pa)	Gas Flow (sccm)	DC_{bias} (V)	Deposition time (min)	Thickness (nm)
BG2	100% Ar	0.3	45	1.8	70	510
BG4	93%Ar + 7%O_2	0.3	45	1.9	70	380
BG5	80%Ar + 20%O_2	0.3	45	0.9	70	330

Advance diffractometer, in parallel beam setting, equipped with copper anode X-ray tube. The measurements were performed in grazing incidence geometry (GIXRD) in order to enhance the signal that stems from the layer. The incidence angle was set to 2°, and the scattered intensity was scanned in the range 5–65° (2θ), with a step size of 0.04°, and 38 s per step.

c. The infrared spectra of the films on the substrates were obtained by Fourier transform infrared spectroscopy (FTIR, model *Mattson Galaxy S-7000*, USA) in diffusion reflectance mode. The analysis was performed within the range 400–4000 cm^{-1}, with a 4 cm^{-1} resolution, with a total of 32 scans per experiment.

d. The surface morphology of the films was examined using scanning electron microscopy (*FE-SEM Hitachi S-4100*, Japan; 25 kV acceleration voltage and 10 μA beam current) under secondary electron mode.

The chemically grown layer thickness was estimated by environmental scanning electron microscopy measurements (ESEM, model *Philips XL30)*. The analysis was performed at an acceleration voltage of 25 kV, in tilt mode; the tilt angle was 30 degrees.

e. The semi-quantitative chemical composition of the as deposited samples was determined by energy dispersive microanalysis (EDS, with a *Bruker-AXS 133eV XFlash® 4010 Detector* attachment)."

f. The adhesion strength at the substrate–film interface was measured by pull-out method, using a certified adhesion tester—PAThandy model (PAT_{handy} *DFD Instruments*, maximum pull force = 6.3 kN), equipped with 2.8 mm diameter stainless steel test elements (stubs). The test method is in accordance with ASTM D4541. The test elements were glued onto the film's surface with a cyanoacrylate one-component epoxy adhesive, E1100S. The stub surface was first polished, ultrasonically degreased in acetone and ethanol and then dried in nitrogen flow. After gluing, the samples were placed in an oven for thermal curing (130°C/h). The pull force was smoothly increased until fracture occurred.

3 Results and discussions

3.1 Thickness determination

The deposition conditions of the BG films are displayed in Table 1. This includes also the films' thickness values estimated by the Swanepoel procedure [28]. This method is based on optical transmittance measurements in the non-absorbance and low absorption region, for films deposited onto glass substrates, in parallel with those deposited on titanium. It can be seen that the film thickness decreases with increasing oxygen pressure in the working chamber. This behavior can be explained by the phenomenon of "target poisoning" induced by chemisorption and ion implantation of oxygen [29–32]. During the sputtering process the BG target is bombarded by ions from the plasma, including reactive oxygen ions. This leads to the formation of a compound film not only on the substrate as desired, but also on the sputtering target. This results in a significantly reduced sputter yield, and thereby, a reduced deposition rate. When increasing the reactive gas flow the degree of target poisoning increases, the sputter erosion rate substantially reduces, and the deposition rate monotonically decreases.

3.2 Pull-out adhesion measurements

In order to estimate the adhesion of the as-sputtered films we tested three samples per condition, and a statistical estimation was performed. The test stub was glued in the center of each sample surface. Failure always occurred at the substrate-film interface, the film being ruined each time. The pull-out strength varied between 70 and 80 MPa with no relevant differences between the BG samples obtained in different conditions. Thus an average adhesion value of ~75 MPa was estimated (small statistic for the moment) for the three types of films.

This adhesion value is much higher than the usual ones reported in literature [9, 17, 18]. These high values of pull-out strength could be attributed to the sputter cleaning and ion bombarding processes of the substrate, done prior to deposition [33, 34]. As it is known, the poor adhesion of the coatings could be ascribed to the natural oxide layers present on the titanium alloy surface before deposition, which leads to poor bonding at the coating–substrate interface.

3.3 SEM–EDS characterization

Figure 1a–c displays scanning electron micrographs of the surface of the as-deposited BG films. The general surface images recorded at a magnification of ×4000 revealed a well-densified, homogeneous surface microstructure, for all types of as-deposited samples. No micro-cracks or delaminations were noticed.

The EDS results of the as-deposited samples are presented in Table 2. The results for the lightest elements (boron and fluorine) were not included because of their expected lower accuracy. Even considering the low accuracy of EDS analysis, the obtained results reveal that there was a clear enrichment of deposited BG4 films in sodium, along with a depletion in calcium. The reason for this non-monotonous evolution of sodium and calcium with

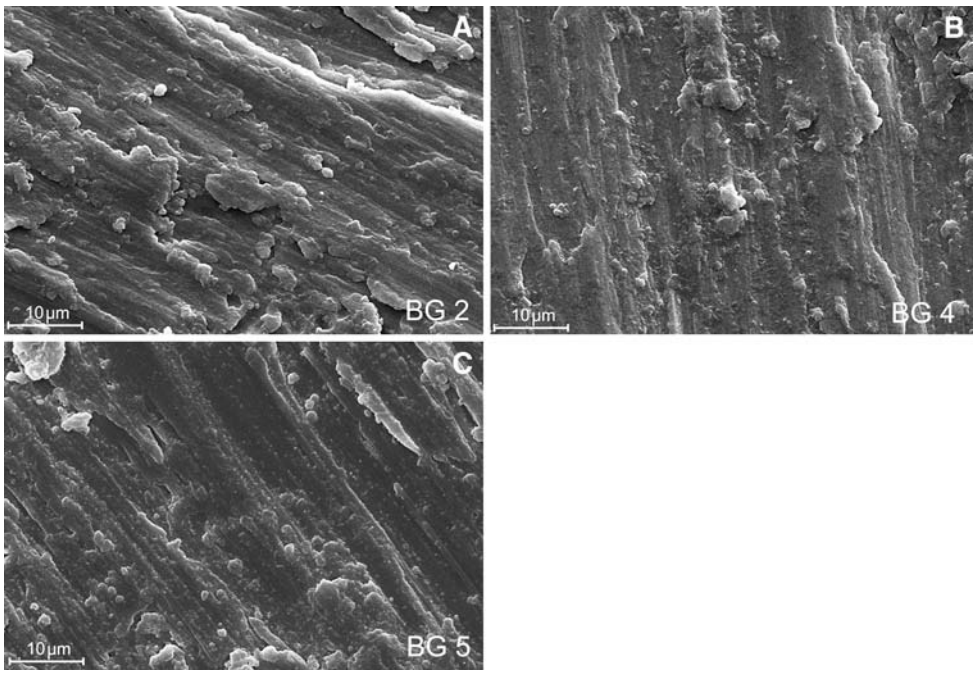

Fig. 1 Top view SEM images of as-deposited bio-glass MS films

increasing oxygen content in the working atmosphere still needs to be better understood, requiring a more systematic approach to clarify it in the future.

The SEM microstructures of the BG2, BG4 and BG5 samples immersed for 30 days are shown in Fig. 2a–c. It can be seen that precipitation of thick and rough coatings occurred for all three types of samples. The chemically deposited layer surface shows spherulitic aspect for all the samples, which is a feature specific to in vitro chemically grown HA [7, 8, 35, 36]. The surface of BG2 and BG4 samples presents regular, spiked spherulitic grains with diameters ranging from 1.7 to 2.4 μm. The BG5 sample surface displays a different topographic aspect with irregularly shaped micro-sized agglomerates and also smoother regions. This suggests that BG2 and BG4 exhibit better mineralization capability, inducing the formation of extensive apatitic layers onto their surfaces. This capability seems to be somewhat lower in the case of BG5.

In order to estimate the thickness of the chemically grown apatitic layers, the films were scratched up to the titanium substrate, and then an ESEM analysis was performed in scratch at a tilt angle of 30° (Fig. 3a–c). The BG4 structure lead to the thickest chemical growth: total film thickness from 2.3 to 3.9 μm, compared to the initial BG thickness of ∼0.4 μm. The BG2 layer increased after 30 days SBF immersion from ∼0.5 μm to 0.7–1.7 μm, while BG5 from ∼0.3 μm up to around 1.2 μm. Thus, the best biomineralization, correlated with the largest thickness of HA layer growth, was obtained for the BG4 coating. The results are in agreement with the FTIR and XRD analysis presented herein.

Table 2 EDS chemical composition in at% calculated for the as deposited BG films

Element	BG2	BG4	BG5
Si	30.2	20.6	31.2
Ca	32	19.8	26.5
P	2.6	2.8	3.9
Na	16.2	26.9	20.6
Mg	19	19.9	17.8

3.4 GIXRD analysis

XRD revealed that the as-deposited structure is amorphous, within the sensitivity limit of the measurement. After 30 days of SBF immersion, all three samples show the characteristic lines of hydroxyapatite, as large, overlapping peaks. The broadening of the HA peaks is probably due both to the very fine crystallite size, and to lattice disorder. Because of the large line broadening, one cannot distinguish between several HA-similar structures, having closely positioned XRD lines. It is generally accepted that the calcia-phosphate-rich layer on the surface is formed by precipitation of calcium and phosphate ions released from the glass together with those from solution, and by incorporating carbonate anions from solution crystallizes into carbonated hydroxyapatite (CHA) [19]. So, we can presume that the preponderant crystalline phase is carbonate hydroxylapatite—$Ca_{10}(PO_4)_3(CO_3)_3(OH)_2$ (ICDD card no. 19-272), which is in agreement with the presence of carbonate groups revealed by FTIR. It is to note that the (002)

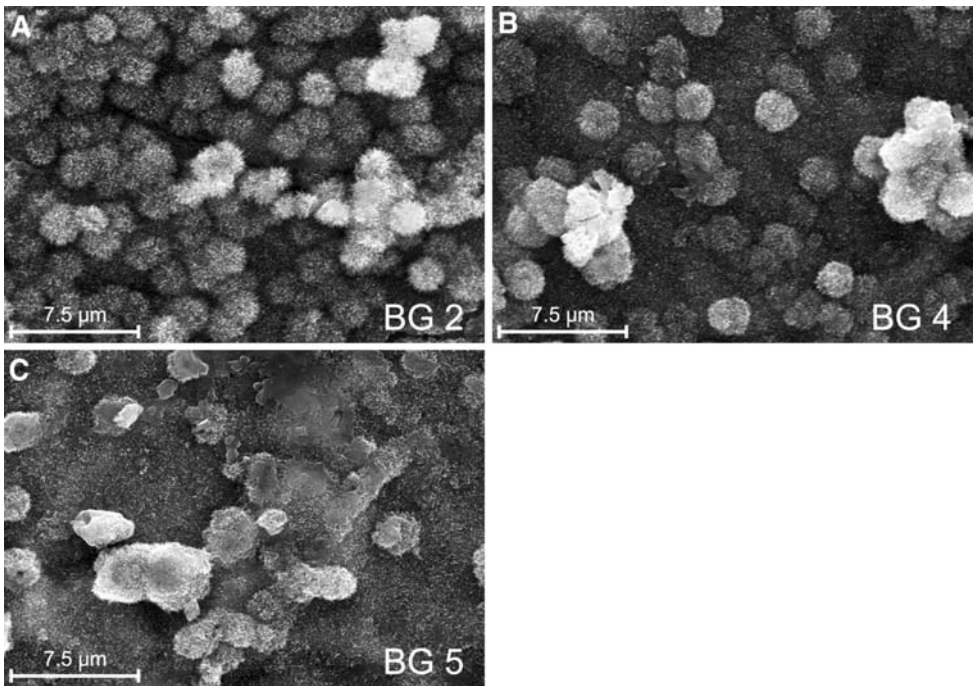

Fig. 2 Top view SEM images of bio-glass MS films after immersion in SBF for 30 days

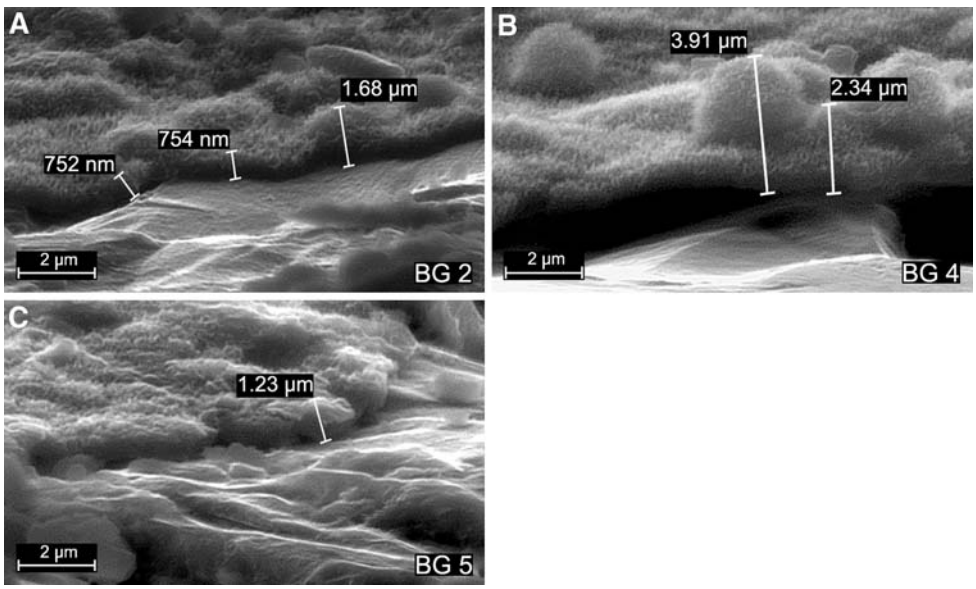

Fig. 3 Tilt view ESEM images of bio-glass MS films after immersion in SBF for 30 days

line of CHA ($2\theta \approx 26°$) has a significantly increased relative intensity compared to the referred ICDD file. This is often observed in HA films and it is generally assigned to the oriented growth of the HA crystallites with respect to the substrate surface.

The XRD patterns (Fig. 4) of BG2 and BG5 also evidence a weak line at $2\theta = 26.4°$, which agrees well with the most intensive line of quartz-like crystalline silica. Besides, there is also a narrow line at $2\theta \approx 36^{\circ}$, that is probably connected to the substrate, and which we assigned to titanium hydride—TiH (ICDD card no. 44-1217), or $TiH_{1.7}$ (ICDD card no. 78-2215). The silica line is not visible in BG4. The penetration depth (90% attenuation) of the X-rays in a HA layer (assuming $\rho_{HA} = 3$ g/cm^3), measured at 2° incidence angle and $2\theta = 26°$ scattered angle, is around 3 μm. Thus, taking into account that the values of the films thickness obtained by tilt ESEM measurement are around 1 μm for BG2 and BG5, and around 3 μm for BG4, one can suppose that the observed SiO_2 line originates from a layer which lies at the bottom side of the chemically deposited layer, thereby its signal is attenuated in the covering HA layer. In the case of BG4, the absence of SiO_2 signal could be explained by the higher thickness of the chemically grown HA film. It is to note that the Ti

substrate lines are visible because there are uncoated regions.

The mechanism of HA formation onto the surface of bioactive glasses is widely accepted [8, 19, 37–40], and involves the dissolution of cations from the surface of bioactive materials and the consequent increase of the supersaturation degree in the surrounding fluid, with respect to HA components. The simultaneous dissolution of silicates results in the formation of silanol groups onto the surface of bio-glasses, which are essential nucleation sites for HA formation. During the dissolution process that precedes the precipitation of calcia and phosphate ions, the hydrated silica (SiOH) which forms on the glass surface undergoes rearrangement by polycondensation of neighboring silanols, resulting in a silica-rich layer. The mechanism of nucleation and growth of the CHA layer is accelerated by the presence of hydrated silica. Our GIXRD and SEM results are consistent with this theory. It seems that this silica-rich bottom layer comprises a quartz-like crystalline phase.

In conclusion: during this dissolution–reprecipitation process the sputtered BG layer is partially dissolved and finally we obtain a multilayer structure containing a bottom BG layer coated by a quartz-like crystalline thin film and at the top a carbonated thick film with HA-like crystalline structure.

3.5 FTIR studies

Figure 5 shows the infrared absorption spectra of the as sputtered bio-glass films together with the spectrum of target powder. All spectra feature a broad absorption band with two peaks at 1010 cm^{-1} (Si–O stretching vibration)

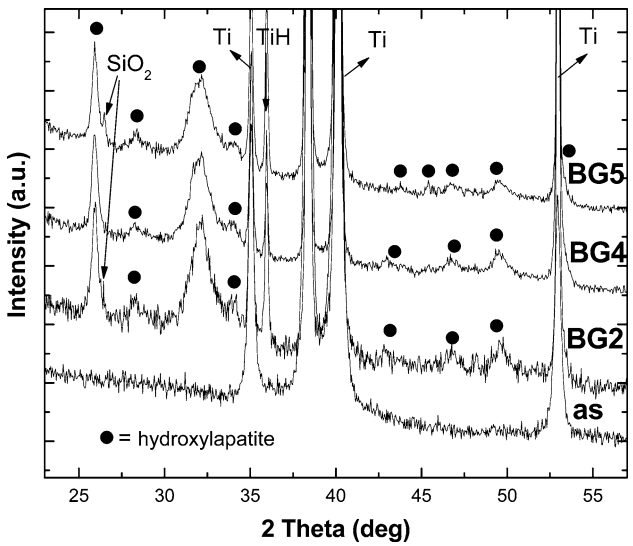

Fig. 4 GIXRD patterns of the as deposited and the in vitro tested samples

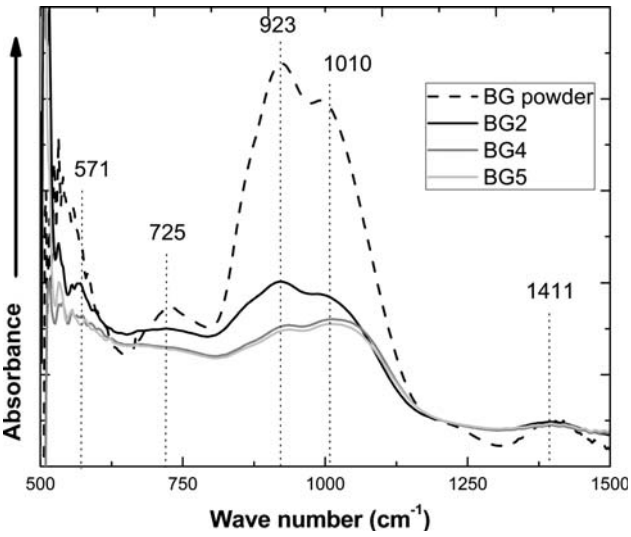

Fig. 5 FTIR spectra for BG target powder and BG as deposited coatings

and 923 cm^{-1} (Si–O–2NBO). Two weaker shoulders were found at lower frequencies: at 571 cm^{-1} (Si–O–Si rocking motion) and at 725 cm^{-1} (Si–O–Si bending motion), respectively. A large vibration band was evidenced centered at 1410 cm^{-1}, most probably due to the vibration of metaborate triangles. Previous IR studies noticed also the presence of Q^2, Q^1, and Q^0 phosphate units in the 1400–400 cm^{-1} IR spectra range [7, 20, 22].

Figure 6 shows the FTIR spectra after 30 days of immersion displaying strong signals of a calcium phosphate phase, identified above as hydroxyapatite by GIXRD characterizations.

The FTIR absorbance spectra of the chemically grown HA films (Fig. 6) revealed strong vibrations at the following wave numbers: 483, 571, 612, 742, 876, 1034 and 1100 cm^{-1}. These absorption bands could be assigned to bending mode of PØP Q^3, Q^2, Q^1 and Q^0 units (550–600 cm^{-1}) and to symmetric stretching bands of PØP Q^3, Q^2 and Q^1 units (650–800 cm^{-1}), respectively. The splitting of the stretching IR absorption band into two narrow components, at 1034 and 1100 cm^{-1}, suggests a crystalline HA growth. These sharp bands correspond to the v_3 asymmetric stretching of the phosphate groups (Table 3).

All grown HA layers were obtained hydroxylated and carbonated as demonstrated by the presence of the strong O–H and $(CO_3)^{2-}$ bands, as follows (Fig. 6; Table 3):

- OH: libration's band at 742 cm^{-1}, v_4 bending vibration present at 1635 cm^{-1}, and a broad band positioned in the 3200–3500 cm^{-1} range;
- CO_3^{2-}: bending vibration band positioned at 876 cm^{-1} and two sharp stretching lines at 1413 cm^{-1} and 1465 cm^{-1}.

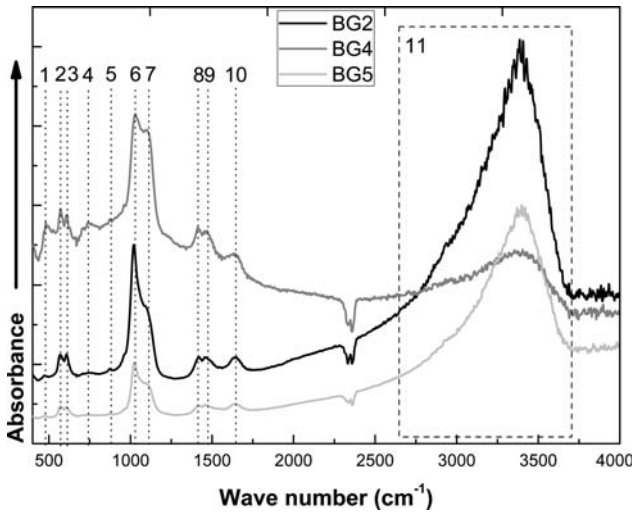

Fig. 6 FTIR spectra for BG coatings immersed in SBF for 30 days (for numeric labels see Table 3)

Figure 7 displays a comparison of $(PO_4)^{3-}$ stretching band integral area of BG films immersed for 30 days. This area can be roughly expressed as a product of the absorption coefficient in the region of stretching vibrations and the number of $(PO_4)^{3-}$ radicals which absorb the infrared light. Considering that most of these phosphate ions belong to hydroxyapatitic structures, the integral area of stretching band is an indicator of the HA layer's mass grown. This area should be proportional to the film thickness in case this would cover the entire substrate surface. After 30 days of soaking in SBF, the original layer partly disappeared, due probably to dissolution or delamination, leaving some uncovered areas on titanium. Thus, the surface covered by the CHA layer differs from sample to sample, and it is difficult to be evaluated. None the less the maximum thickness value estimated by ESEM for BG4 structure is concordant with the infrared and XRD results.

The degree of hydroxylation expressed as (OH area/PO_4 area) is also displayed in Fig. 7. This parameter is not dependant on the covering percent, so it provides useful information upon the chemically grown films structure. It suggests that the highest degree of bioactivity (maximum CHA thickness) is obtained in the case of BG4 film which is also the less hydroxylated one. The highest values of hydroxylation degree were obtained for BG2 and BG5 films, proving their lower degrees of in vitro bioactivity in SBF.

Hench's theory states that the first stage of a bio-glass mineralization upon immersion in SBF involves the rapid exchange of Na^+ ions from the glass for H^+ and H_3O^+ ions

Table 3 Assignment of IR vibration bands for the immersed BG structures

No.	Position	Vibration band
1	483	O–P–O (v_2) bending mode
2	571	$(PO_4)^{3-}$ (v_4) asymmetric bending mode
3	612	$(PO_4)^{3-}$ (v_4) asymmetric bending mode
4	742	Si–O–Si bending mode, O–H libration mode
5	876	$(CO_3)^{2-}$ (v_2) asymmetric bending mode
6	1034	$(PO_4)^{3-}$ (v_3) asymmetric stretching mode
7	1100	SiO_2 strong streching vibration band, (PO_3) (v_3) mode in Q^2 units
8	1413	$(CO_3)^{2-}$ (v_3) asymmetric stretching mode
9	1465	$(CO_3)^{2-}$ (v_3) asymmetric stretching mode
10	1635	O–H bending mode
11	3200–3500	O–H streching mode

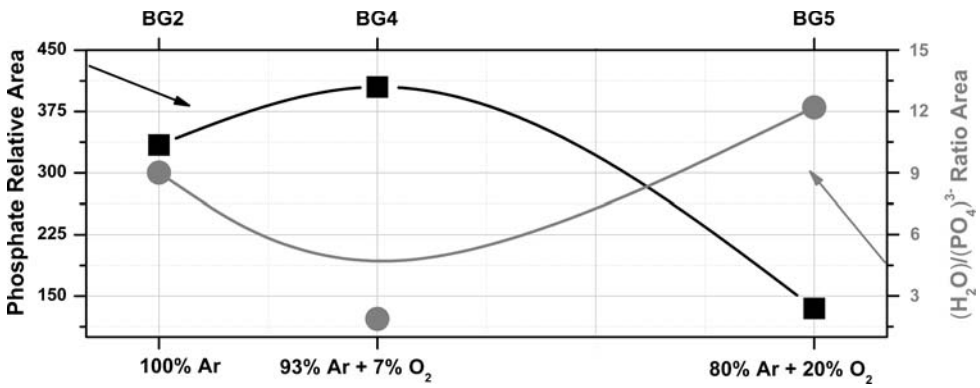

Fig. 7 Integral area of stretching band $(PO_4)^{3-}$ (*left*); degree of hydroxylation expressed as H_2O area/PO_4 area (*right*) for BG films after 30 days of immersion

from the solution, which shall initialize the hydrolysis of the Si–O–Si bonds of the glass structure and the forming of silanol groups. In a next step the silanol groups polycondensate forming a silica-rich layer at the bio-glass surface, which favors the growth of Ca–P type layers. Therefore, one can speculate that the higher biomineralization rate of BG4 film is due to an acceleration of the chemical processes involved in the so called Hench's mechanism because of the higher sodium content of this film (Table 2). The higher number of sodium ions released in SBF will change the chemical equilibrium of the precipitation reaction accelerating the hydrolysis of silicon–oxygen–silicon bonds, thereby catalyzing the formation and chemical growth of CHA. We are therefore assuming that different Na/Ca ratios will lead to different biomineralization behaviors. Although releasing Ca ions in SBF is of great importance to supersaturate the solution with respect to HA composition, thus favoring the precipitation of Ca–P compound, a higher content of Na ions in the bio-glass film leads to a faster hydration of silica, speeding up the chemical growth of CHA.

4 Conclusions

Highly adherent sputtered films have been successfully deposited onto Ti substrates using RF magnetron method in inert and reactive atmospheres. All three types of films (BG2-Ar 100%, BG4-Ar + 7%O_2, BG5-Ar + 20%O_2) showed pronounced bioactivity when soaked in SBF. Micrometric carbonated hydroxyapatite rough coatings were obtained after 30 days SBF soaking, as proved by the SEM, GIXRD and FTIR results. GIXRD patterns of the soaked films also evidenced the presence of a quartz-like SiO_2 phase for BG2 and BG5 (as a weak line at $2\theta = 26.4°$), which is probably grown below the CHA structure. The absence of the quartz line in BG4 pattern can be explained by the thicker chemically grown CHA layer, which exceeds the X-rays attenuation limit. FTIR spectra displayed a strong hydroxylation and carbonatation phenomena of these calcium phosphate coatings which are typical for chemically grown and biological apatites. The chemically grown coatings' quality strongly depended on the "seed" bio-glass sputtered films, the highest thickness and the lowest hydroxylation rate being obtained in the case of the BG4 structure. One can speculate that the presence of a higher content of sodium in the bio-glass films leads to faster hydration of silica, speeding up the other chemical growth stages of CHA. The other structures, BG2 and BG5, had thinner chemically grown CHA layers, which proved to be more hydroxylated than in case of BG4. The above results are concordant with the SBF dissolution–reprecipitation model of Hench.

The high values of adhesion and strong SBF bioactivity after 30 days encourage us to continue with more detailed SBF studies to deeply understand the physical–chemical processes implied in the chemical grown phenomena.

Acknowledgments Thanks are due to CICECO for the support and to the Portuguese Foundation for Science and Technology for the fellowship grants of S. Pina (SFRH/BD/21761/2005) and to Romanian Ministry of Education and Research for the scientific projects support: CEEX 307/2006 and PN II 71-110/2007. The financial support of "BD" PhD research scholarship offered by CNCSIS is also gratefully acknowledged by G.E. Stan.

References

1. Lossdorfer S, Schwartz Z, Lohmann CH, Greenspan DC, Ranly DM, Boyan BD. Osteoblast response to bioactive glasses in vitro correlates with inorganic phosphate content. Biomaterials. 2004; 25:2547–55.
2. Cerruti M, Greenspan D, Powers K. Effects of pH and ionic strength on the reactivity of Bioglass® 45S5. Biomaterials. 2005; 26:1665–74.
3. Saranti A, Koutselas I, Karakassides MA. Bioactive glasses in the system $CaO–B_2O_3–P_2O_5$: preparation, structural study and in vitro evaluation. J Non-Cryst Solids. 2006;352:390–8.
4. Andrade AL, Valério P, Goes AM, de Fatima Leite M, Domingues RZ. Influence of morphology on in vitro compatibility of bioactive glasses. J Non-Cryst Solids. 2006;352:3508–11.
5. Chen QZ, Thompson ID, Boccaccini AR. 45S5 Bioglass (R)-derived glass-ceramic scaffolds for bone tissue engineering. Biomaterials. 2006;27(11):2414–25.
6. Yan X, Huang X, Yu C, Deng H, Wang Y, Zhang Z, et al. The in vitro bioactivity of mesoporous bioactive glasses. Biomaterials. 2006;27:3396–903.
7. Agathopoulos S, Tulyaganov DU, Ventura JMG, Kannan S, Karakassides MA, Ferreira JMF. Formation of hydroxyapatite onto glasses of the $CaO–MgO–SiO_2$ system with B_2O_3, Na_2O, CaF_2 and P_2O_5 additives. Biomaterials. 2006;27:1832–40.
8. Balamurugan A, Balossier G, Kannan S, Michel J, Rebelo AHS, Ferreira JMF. Development and in vitro characterization of sol–gel derived $CaO–P_2O_5–SiO_2–ZnO$ bioglass. Acta Biomater. 2007;3:255–62.
9. Mardare CC, Mardare AI, Fernandes JRF, Joanni E, Pina SCA, Fernandes MHV, et al. Deposition of bioactive glass-ceramic thin-films by RF magnetron sputtering. J Eur Cer Soc. 2003;23: 1027–30.
10. Lopez-Esteban S, Saiz E, Fujino S, Oku T, Suganuma K, Tomsia AP. Bioactive glass coatings for orthopedic metallic implants. J Eur Cer Soc. 2003;23:2921–30.
11. Liste S, Serra J, Gonzalez P, Borrajo JP, Chiussi S, Leon B, et al. The role of the reactive atmosphere in pulsed laser deposition of bioactive glass films. Thin Solid Films. 2004;453–454:224–8.
12. Izquierdo-Barba I, Conde F, Olmo N, Lizarbe MA, Garcia MA, Vallet-Regi M. Vitreous SiO2–CaO coatings on Ti6Al4 V alloys: reactivity in simulated body fluid versus osteoblast cell culture. Acta Biomater. 2006;2:445–55.
13. Borrajo JP, Serra J, Gonzalez P, Léon B, Munoz FM, Lopez M. In vivo evaluation of titanium implants coated with bioactive glass by pulsed laser deposition. J Mater Sci Mater Med. 2007;18: 2371–6. doi:10.1007/s10856-007-3153-z.
14. Fathi MH, Doost Mohammadi A. Preparation and characterization of sol–gel bioactive glass coating for improvement of

biocompatibility of human body implant. Mater Sci Eng A. 2008;474:3–128.
15. Zhao Y, Song M, Chen C, Liu J. The role of the pressure in pulsed laser deposition of bioactive glass films. J Non-Cryst Solids. 2008;354:4000–4.
16. Berbecaru C, Alexandru HV, Ianculescu A, Popescu A, Socol G, Sima F, et al. Bioglass thin films for biomimetic implants. Appl Surf Sci. 2009;255(10):5476–9.
17. Peddi L, Brow RK, Brown RF. Bioactive borate glass coatings for titanium alloys. J Mater Sci Mater Med. 2008;19:3145–52. doi:10.1007/s10856-008-3419-0.
18. Goller G. The effect of bond coat on mechanical properties of plasma sprayed Bioglass-titanium coatings. Ceram Int. 2004;30: 351–5.
19. Hench LL, Wilson J. An introduction to bioceramics. 1st ed. Singapore: World Scientific Publishing Company; 1993.
20. Saiz E, Tomsia AP, Fujino S, Gomez-Vega JM. Graded coatings for metallic implant alloys. In: Lewinsohn CA, Singh M, Loehman R, editors. Ceramic transactions: advances in joining of ceramics. 2000. p. 159–72.
21. Wasa K, Kitabatake M, Adachi H. Thin film materials technology: sputtering of compound materials. New York: Noyes Publications; 2003.
22. Agathopoulos S, Tulyaganov DU, Valério P, Ferreira JMF. A new model formulation of the SiO_2–Al_2O_3–B_2O_3–MgO–CaO–Na_2O–F glass-ceramics. Biomaterials. 2005;26:2255–64.
23. Agathopoulos S, Tulyaganov DU, Ventura JMG, Kannan S, Saranti A, Karakassides MA, et al. Structural analysis and devitrification of glasses based on the CaO–MgO–SiO_2 system with B_2O_3, Na_2O, CaF_2 and P_2O_5 additives. J Non-Cryst Solids. 2006;352:322–8.
24. Tulyaganov DU, Agathopoulos S, Ventura JMG, Karakassides MA, Fabrichnaya O, Ferreira JMF. Synthesis of glass–ceramics of CaO–MgO–SiO_2 system containing B_2O_3, P_2O_5, Na_2O and CaF_2. J Eur Cer Soc. 2006;26:1463–71.
25. Tulyaganov DU, Agathopoulos S, Fernandes HR, Ferreira JMF. Processing of glass-ceramics in the SiO_2–Al_2O_3–B_2O_3–MgO–CaO–Na_2O–(P_2O_5)–F system via sintering and crystallization of glass powder compacts. Ceram Int. 2006;32:195–200.
26. Epple M, Bäuerlein E. Handbook of biomineralization: medical and clinical aspects. NY: Wiley; 2009.
27. Kokubo T, Kushitani H, Ohtsuki C, Sakka S, Yamamuro T. Effects of ions dissolved from bioactive glass-ceramic on the surface apatite formation. J Mater Sci Mater Med. 1993;4:1–4.
28. Swanepoel RJ. Determination of the thickness and optical constants of amorphous silicon. J Phys E Sci Instrum. 1983;16: 1214–22.
29. Güttler D, Abendroth B, Grötzschel R, Möller W, Depla D. Mechanisms of target poisoning during magnetron sputtering as investigated by real-time in situ analysis and collisional computer simulation. Appl Phys Lett. 2004;85(25):6134–6.
30. Rosen D. Defining the surface binding energy in dynamic Monte Carlo simulation for reactive sputtering of compounds. Vacuum. 2006;80:944–8.
31. Berg S, Nyberg T. Fundamental understanding and modeling of reactive sputtering processes. Thin Solid Films. 2005;476(2): 215–30.
32. Rosen D, Katardjiev I, Berg S, Moller W. TRIDYN simulation of target poisoning in reactive sputtering. Nucl Instrum Methods Phys Res B. 2005;228:193–7.
33. Ding SJ. Properties and immersion behavior of magnetron-sputtered multilayered hydroxyapatite/titanium composite coatings. Biomaterials. 2003;24:4233–8.
34. Stan GE, Morosanu CO, Marcov DA, Pasuk I, Miculescu F, Reumont G. Effect of annealing upon the structure and adhesion properties of sputtered bio-glass/titanium coatings. Appl Surf Sci. 2009;255:9132–8.
35. Juhasz JA, Best SM, Auffret AD, Bonfield W. Biological control of apatite growth in simulated body fluid and human blood serum. J Mater Sci Mater Med. 2008;19(4):1823–9.
36. Stan GE, Ferreira JMF. An algorithm for preparing bioactive fluorinated hydroxyapatite coatings by sol gel technique. J Optoelectron Adv Mater. 2007;9(8):2539–42.
37. Hench LL. Bioceramics: from concept to clinic. J Am Ceram Soc. 1991;74:1487–510.
38. Hench LL. The story of Bioglass®. J Mater Sci Mater Med. 2006;17:967–78. doi:10.1007/s10856-006-0432-z.
39. Kim CY, Clark AE, Hench LL. Early stages of calcium-phosphate formation in bioglasses. J Non-Cryst Solids. 1989;113: 195–202.
40. Hill R. An alternative view of the degradation of bioglass. J Mater Sci Lett. 1996;15:1122–5.